Bone histology of acipenseriform fishes reveals seasonality during the final years of the Mesozoic.

Jan Smit (j.smit@vu.nl)
VU University Amsterdam
Melanie During
Uppsala University
Camille Berruyer
European Synchrotron Radiation Facility
Dennis Voeten
European Synchrotron Radiation Facility https://orcid.org/0000-0002-2090-2824
Paul Tafforeau
European Synchrotron Radiation Facility https://orcid.org/0000-0002-5962-1683
Sophie Sanchez
Uppsala University https://orcid.org/0000-0002-3611-6836
Susan Verdegaal Warmerdam
Vrije Universiteit
Jeroen van der Lubbe
Faculty of Science, Vrije University https://orcid.org/0000-0001-7545-6502

Biological Sciences - Article

Keywords: Cretaceous-Paleogene (KPg), exstinction, seasonality

Posted Date: July 12th, 2021

DOI: https://doi.org/10.21203/rs.3.rs-646564/v1

Version of Record: A version of this preprint was published at Nature on February 23rd, 2022. See the published version at https://doi.org/10.1038/s41586-022-04446-1.

Bone histology of acipenseriform fishes reveals seasonality during the final years of the Mesozoic.

Melanie A. D. During[1,2], Jan Smit[1*], Camille Berruyer[3], Dennis F. A. E. Voeten[3], Paul Tafforeau[3], Sophie Sanchez[2,3], Suzan Verdegaal-Warmerdam[1] & Jeroen (H) J. L. van der Lubbe[1,4]

[*]j.smit@vu.nl

[1]Department of Earth Sciences, Faculty of Science, Vrije Universiteit Amsterdam, De Boelelaan 1085, 1081HV Amsterdam, the Netherlands

[2]Subdepartment of Evolution and Development, Department of Organismal Biology, Evolutionary Biology Centre, Uppsala University Norbyvägen 18A, 752 36 Uppsala, Sweden

[3]European Synchrotron Radiation Facility, 71 Avenue des Martyrs, CS-40220, 38043 Grenoble Cedex, France

[4]School of Earth and Ocean Sciences, Cardiff University, Main Building, Park Place, Cardiff, CF10 3AT, United Kingdom

The Cretaceous-Paleogene (KPg) mass extinction ~66 million years ago (Ma) was triggered by the Chicxulub impact on the present-day Yucatán Peninsula. This event caused the extinction of circa 76% of species[1], including all non-avian dinosaurs, and represents one of the most selective extinctions to date. The timing of the impact and its aftermath have mainly been studied on millennial timescales, leaving the season of the impact unconstrained. Here, we demonstrate that the impact that caused the KPg mass extinction took place during boreal spring. Osteohistology and stable isotope records of exceptionally preserved dermal and perichondrial bones in acipenseriform fishes from the Tanis impact-induced seiche deposits[2] reveal annual cyclicity across the final years of the Cretaceous. These fishes ultimately perished in boreal spring. Annual life cycles, involving seasonal timing and duration of reproduction, feeding, hibernation, and aestivation, vary strongly across latest Cretaceous biotic diversity. We conclude that the timing of the Chicxulub impact in boreal spring significantly influenced selective biotic survival across the KPg boundary.

The discovery of a globally distributed iridium anomaly caused by to the Chicxulub impact ~66 (Ma) fuelled discussions on the causal mechanisms behind the Cretaceous-Paleogene (KPg) mass extinction[3,4,5,6]. This extinction event affected biodiversity with high but poorly understood taxonomic selectivity. Among archosaurs, for example, all pterosaurs and non-avian dinosaurs succumbed in the KPg mass extinction while crocodilians and birds survived into the Paleogene. Direct consequences of the impact, including returning impact glass spherules, large-scale forest fires, and tsunamis, are geologically documented >3500 km from the Yucatán impact crater[7,2]. Although direct effects of the impact devastated vast proximal geographical areas, the global mass extinction likely unfolded during its aftermath, which is estimated to have resulted in rapid climate change, lasting up to several thousands of years[8,9].

The Tanis event deposit in North Dakota (USA) is an exceptional seiche deposit preserving a rich thanatocoenosis (i.e. a mass death assemblage) of latest Cretaceous biota. The majority of macrofossils encountered at the Tanis locality represent direct casualties of the KPg bolide impact that were buried within the impact-induced seiche deposit[2]. Tens of minutes after the impact, the seiche agitated large volumes of water and soil upstream on the estuary of the Tanis river[2,10]. As the seiche ran up the estuary it led to the admixing of bones, teeth, bivalves, ammonites, benthic foraminifera, and plant matter while impact spherules rained down from the sky[2]. Within the thanatocoenosis, abundant acipenseriformes – sturgeons and paddlefishes – were oriented along the seiche flow directions and buried alive with numerous impact spherules in their gills[2] (Figure 1).

R. DePalma suggested (pers. comm.) that indications for the season of the Chicxulub impact could be preserved within the Tanis seiche deposit. To uncover the season of the KPg bolide impact, we analysed paddlefish dentaries and sturgeon pectoral fin spines that were excavated at the Tanis site in 2017. These skeletal elements preserve an unaltered growth record from embryonic development up to death, rendering them highly suitable for life history reconstructions[11,12]. Tanis was located at approximately at 50° N during the latest Cretaceous and experienced a distinct seasonality in rainfall and temperature[13]. Regional air temperatures were reconstructed to range from 4-6 °C in winter up to an average of ~19 °C in summer[13,14]. In the latest stage of Cretaceous (i.e. the Maastrichtian), the climate of present-day North Dakota involved four seasons that can be traced in the acipenseriform skeletal elements (Figure 2; Supplementary information 1) as well as in contemporaneous tree records from the nearby Hell Creek Formation[14,15].

We here combined micrometre-resolution records of acipenseriform bone apposition with an incremental carbon isotope record to reconstruct seasonal growth and identify the season during which the KPg bolide impacted. We used propagation-based phase-contrast synchrotron radiation micro-computed tomography (PPC-SR µCT) on beamline BM05 at the European Synchrotron Radiation Facility[16] to visualise a partial paddlefish skeleton in

3D and disclose the osteohistology of acipenseriform bones. These tomographic data show that impact spherules associated with the paddlefish skeleton are exclusively present in its gill rakers[2] and are absent elsewhere in the preserved specimen (Figure 1). The absence of impact spherules outside the gill rakers demonstrates that they did not yet proceed into the oral cavity or further down the digestive tract, nor that they impacted the fish remains during perimortum exposure. Impact spherule accumulation in the gill rakers and arrival of the seiche must thus have occurred virtually instantaneously[2], indicating that the acipenseriforms were alive during the bolide impact and the last minutes of the Cretaceous.

The degree of preservation of sampled acipenseriform bones was assessed using micro X-ray fluorescence (µ-XRF, see Methods; Supplementary information 2), which is capable of revealing potential taphonomic elemental exchange that may have affected the primary stable isotope composition. The µXRF maps show that Fe- and Mn-oxides are present in the bone vascular canals and surrounding sediments, but have not invaded the bone apatite. Detrital sediments, characterised by high concentrations of K and Si, remain restricted to the sediment matrix. The bone apatite conserves a highly homogeneous distribution of P and Ca, which corroborates the unaltered preservation of these apatitic tissues. Skeletal remains of these paddlefishes and sturgeons thus experienced negligible diagenetic alteration, likely due to their rapid burial and possibly aided by early Mn and Fe oxide seam formation[17,18]. The three-dimensional preservation of delicate structures, including non-ossified tissues that originally enveloped the brain (Supplementary Information 3), further demonstrates the excellent preservation of the fossil and absence of taphonomic reorganisation[19].

Like their modern-day relatives, the latest Maastrichtian paddlefishes of Tanis were filter feeders that presumably consumed copepods and other zooplankton[20,21,22]. These fishes likely experienced an annual feeding pattern, determined by fluctuating food availability, which peaks between spring and autumn[20].

Paddlefish dentaries consist of perichondrial bone and sturgeon pectoral fin spines consist of dermal bone – an intramembranous skeletal tissue that formed in the mesenchyme (mesodermal embryonic tissue) and both, unlike endochondral bone, did not originate through ossification of cartilaginous precursors[23,24,25]. Fish dentaries are formed by perichondrial ossification around the Meckel's cartilage[26,27]. Both dermal and perichondrial bone growth exclusively proceeds through incremental bone matrix secretion and apposition by a row of osteoblasts[24,25,26,27,28,29]. The cumulative thickness of one annual growth mark spans a thick (favourable) growth zone, a thinner (slowly-deposited) annulus, and ultimately a line of arrested growth (LAG)[28,29,30]. All bones studied here, representing six acipenseriform individuals, exhibit osteocyte lacunar densities towards their periosteal surfaces that consistently remained lower than highest densities recorded during previous years[31]. This indicates bone growth at the time of death that was not yet slowing down (Figure 2 and Supplementary Materials 1).

The inferred growth histories are independently corroborated by a stable carbon isotope ($\delta^{13}C$) archive that recorded several years of seasonal dietary fluctuations in growing bone. During maximum productivity, the zooplankton is expected to enrich the growing skeleton of filter-feeding fishes with ^{13}C relative to ^{12}C [32,33]. As such, the cyclically elevated $^{13}C/^{12}C$ ratios in paddlefish X-2724 (Figure 2) reflect distinct episodes of high food availability. Carbon isotope records across the growth record of Paddlefish X-2724 indicates that peak annual growth rate was not yet attained and the feeding season had thus not yet climaxed – the conclusive signature of a boreal spring death.

The catastrophic end-Cretaceous bolide impact during the Northern Hemisphere boreal spring places the event in a particularly sensitive phase of biological life cycles. For many taxa, annual reproduction and growth take place during spring. A spring impact would therefore have rendered such taxa particularly vulnerable to extinction. This is especially the case for species with small numbers of offspring and/or long incubation times, such as pterosaurs and non-avian dinosaurs relative to surviving mammals, amphibians, reptiles and

122 birds[34,35,36]. A spring impact confirms the earlier hypothesis by Wolfe[37] who presented
123 palaeobotanical indications for a June impact. The last boreal spring of the Cretaceous quickly
124 gave way to an impact winter, as large amounts of dust and aerosols reduced solar irradiation
125 for decades[38]. Ecological networks collapsed from the bottom up, as floral extinctions directly
126 affected species dependent on primary producers more so than animals that were able to
127 explore alternative resources, such as birds[39,40]. Alongside e.g. the end-Cretaceous
128 distributions of ecological flexibility and metabolic strategy, the timing of the impact therefore
129 potentially contributed to the still poorly understood patterns of selective survival across the
130 KPg boundary

131 The seasonal timing of the Chicxulub impact will aid in explaining the selectivity of
132 the KPg extinction. We further posit that a spring impact will have affected biota in the Northern
133 Hemisphere to a greater extent than an autumn impact in the Southern Hemisphere. This may
134 have caused asymmetry in extinction and recovery patterns between the two hemispheres,
135 partially due to the unequal distributions of terrestrial and marine environments. Although the
136 Northern Hemisphere accommodated most of the terrestrial biota, the differential impact of the
137 extinction on Northern vs. Southern hemisphere ecosystems remains underexplored. The
138 diverse Latest Cretaceous ecosystem recorded at the uniquely-constrained Tanis site will help
139 in reconstructing the environmental, climatological, and biological conditions that locally
140 prevailed when the Mesozoic terminated.

141

142 **References**

143 [1] Lowery, Christopher M., et al. Rapid recovery of life at ground zero of the end-Cretaceous
144 mass extinction. Nature 558, 288- 291 (2018).

145 [2] DePalma, Robert A., et al. A seismically induced onshore surge deposit at the KPg
146 boundary, North Dakota. Proc. Natl. Acad. Sci. USA 116, 8190-8199 (2019).

147 [3] Smit, Jan, and Jan Hertogen. An extraterrestrial event at the Cretaceous–Tertiary
148 boundary. Nature 285, 198-200 (1980).

149 [4] Alvarez, Luis W., et al. Extraterrestrial cause for the cretaceous-tertiary extinction:
150 experiment and theory. Applications of Space Developments. Pergamon, 241-271, (1981).

151 [5] Smit, Jan, et al. Tektite-bearing, deep-water clastic unit at the Cretaceous-Tertiary
152 boundary in northeastern Mexico. *Geology* 20, 99-103 (1992).

153 [6] Alvarez, Walter. Trajectories of ballistic ejecta from the Chicxulub Crater. *The Cretaceous-*
154 *Tertiary Event and Other Catastrophes in Earth History* 307, 141 (1996).

155 [7] Smit, J. The global stratigraphy of the Cretaceous-Tertiary boundary impact ejecta. Annual
156 Review of Earth and Planetary Sciences 27, 75-113 (1999).

157 [8] Morgan, Joanna, et al. Revisiting wildfires at the K-Pg boundary. *J. Geophys. Research:*
158 *Biogeosciences* 118, 1508-1520 (2013).

159 [9] Vellekoop, Johannes, et al. Phytoplankton community disruption caused by latest
160 Cretaceous global warming. Biogeosciences 16, 4201-4210 (2019).

161 [10] Artemieva, Natalia, and Joanna Morgan. Global K-Pg layer deposited from a dust
162 cloud. Geophysical Research Letters, e2019GL086562 (2020).

163 [11] Adams, Leverett A. Age determination and rate of growth in Polyodon spathula, by means
164 of the growth rings of the otoliths and dentary bone. The American Midland Naturalist 28,
165 617-630 (1942).

166 [12] Bakhshalizadeh, Shima, et al. Identifying major events in two sturgeons' life using
167 pectoral fin spine ring structure: exploring the use of a non-destructive
168 method. Environmental Science and Pollution Research 24, 18554-18562 (2017).

169 [13] Hallam, Anthony. A review of Mesozoic climates. J. Geo. Soc. 142, 433-445 (1985).

[14] Golovneva, L. B. The Maastrichtian (Late Cretaceous) climate in the northern hemisphere. Geol. Soc., London, Spec. Pub., 181, 43-54 (2000).

[15] Wolfe, Jack A., and Garland R. Upchurch Jr. North American nonmarine climates and vegetation during the Late Cretaceous. Palaeogeog., palaeoclim., palaeoecol. 61, 33-77 (1987).

[16] Tafforeau, Paul, et al. "Applications of X-ray synchrotron microtomography for non-destructive 3D studies of paleontological specimens." Applied Physics A 83.2 (2006): 195-202.

[17] Hedges, Robert EM. Bone diagenesis: an overview of processes. Archaeometry 44, 319-328 (2002).

[18] Dumont, M., et al. Synchrotron XRF analyses of element distribution in fossilized sauropod dinosaur bones. Powder Diffraction 24, 130-134 (2009).

[19] Pradel, Alan, et al. "Skull and brain of a 300-million-year-old chimaeroid fish revealed by synchrotron holotomography." Proceedings of the National Academy of Sciences 106.13 (2009): 5224-5228.

[20] Blackwell, Brian G., et al. Suitability of food resources and physicochemical parameters in the lower Trinity River, Texas for paddlefish. J. Freshwater Ecology 10, 163-175 (1995).

[21] Bemis, William E., and Boyd Kynard. Sturgeon rivers: an introduction to acipenseriform biogeography and life history. Environmental Biology of Fishes 48, 167-183 (1997).

[22] Rosen, Rudolph S. Distribution, age, and growth, and feeding ecology of paddlefish (Polyodon spathula) in unaltered Missouri River, South Dakota. Theses and Dissertations. 208, (1976).

[23] Grande, Lance, and William E. Bemis. Osteology and phylogenetic relationships of fossil and recent paddlefishes (Polyodontidae) with comments on the interrelationships of Acipenseriformes. J. Vert. Paleo. 11, 1-121 (1991).

195 [24] De Ricqlès, A. J., et al. Bone, Vol. 3, Bone Matrix and Bone Specific Products. 78 (1991).

196 [25] Hall, Brian K. Bones and cartilage: developmental and evolutionary skeletal biology.
197 Elsevier, 2005.

198 [26] Hall, Brian K. Bones and cartilage: developmental and evolutionary skeletal biology.
199 Elsevier, 2005.

200 [27] Weigele, Jochen, and Tamara A. Franz-Odendaal. "Functional bone histology of
201 zebrafish reveals two types of endochondral ossification, different types of osteoblast
202 clusters and a new bone type." Journal of anatomy 229.1 (2016): 92-103.

203 [28] Hirasawa, Tatsuya, and Shigeru Kuratani. Evolution of the vertebrate skeleton:
204 morphology, embryology, and development. Zoological letters 1, 2 (2015).

205 [29] Enlow, D.H., . The Human Face: An Account of the Postnatal Growth and Development
206 of the Craniofacial Skeleton. Harper & Row. 1968

207 [30] LeBreton, Greg TO, F. William H. Beamish, and Scott R. McKinley, eds. Sturgeons and
208 paddlefish of North America. Vol. 27. Springer Science & Business Media, 2006.

209 [31] Sanchez, Sophie, et al. "Three-dimensional synchrotron virtual paleohistology: a new
210 insight into the world of fossil bone microstructures." Microscopy and Microanalysis 18.5
211 (2012): 1095.

212 [32] Fry, Brian, and E. Barry Sherr. δ 13 C measurements as indicators of carbon flow in
213 marine and freshwater ecosystems. Stable isotopes in ecological research. Springer, New
214 York, USA, 196-229 (1989).

215 [33] Finlay, Jacques C. Stable-carbon-isotope ratios of river biota: implications for energy flow
216 in lotic food webs. Ecology 82, 1052-1064 (2001).

[34] Erickson, Gregory M., et al. Dinosaur incubation periods directly determined from growth-line counts in embryonic teeth show reptilian-grade development. *Proceedings of the National Academy of Sciences* 114, 540-545 (2017).

[35] Garcia, C. Macías, E. Saborío, and C. Berea. "Does male-biased predation lead to male scarcity in viviparous fish?." *Journal of Fish Biology* 53 (1998): 104-117.

[36] Efford, I. E., C. Macias Garcia, and J. D. Williams. "Facing the challenges of invasive alien species in North America." *Global Biodiversity Canadian Museum of Nature* 7.1 (1997): 25-30.

[37] Wolfe, Jack A. "Palaeobotanical evidence for a June 'impact winter' at the Cretaceous/Tertiary boundary." *Nature* 352.6334 (1991): 420-423.

[38] Vellekoop, Johan, et al. "Rapid short-term cooling following the Chicxulub impact at the Cretaceous–Paleogene boundary." Proceedings of the National Academy of Sciences 111.21 (2014): 7537-7541.

[39] Field, Daniel J., et al. "Early evolution of modern birds structured by global forest collapse at the end-Cretaceous mass extinction." Current Biology 28.11 (2018): 1825-1831.

[40] Schleuning, Matthias, et al. "Ecological networks are more sensitive to plant than to animal extinction under climate change." Nature Communications 7.1 (2016): 1-9.

Materials and Methods

Fieldwork

The excavation for this study took place from August 10 until August 20, 2017, at the Tanis locality, in southwestern North Dakota. In a team lead by Robert DePalma, we excavated the acipenseriform fishes. Sections of dentaries of paddlefishes and pectoral fin-spines of sturgeons were collected in the field for the histological study.

Thin sectioning

The majority of the samples were separated from the sediment matrix. This included all sturgeon pectoral fin spine samples: X-2743M, X-2744M, MDX-3 and one of the paddlefish dentaries (X-2724). Paddlefish dentary samples X-2733a and X-2733b were fractured. Their exact orientation was unknown and the material was highly unstable. To avoid further fracturing the specimens were embedded in an epoxy resin prior to thin sectioning. All specimens were cut with a diamond saw and polished to obtain the thin sections (~50-micrometer thickness) and thick-sections for micromilling (~200-micrometer thickness).

Micro X-ray Fluorescence

Fragments of the paddlefish and sturgeon samples that remained after thin sectioning have been analyzed by Micro X-ray Fluorescence (μXRF) for elemental mapping at 20 μm/5 milliseconds at 50 kV 600μA 2 spectrometers Rh (rhodium) with no filter at the Vrije Universiteit Brussel (VUB).

Micromill

The growth increments were sampled from the thick sections as accurate as possible using a Micromill (Merkantek). Drill transects were assigned in the accompanying software and per transect every individual sample was collected and the drill bit was cleaned with ethanol. Not all thick-sections were suitable for the micromilling, the lobed structure of the sturgeon specimens proved too curved for the micromill, and paddlefish specimens X-2733a and X-2733b had only a few growth lines that proved too narrow for micromilling. Sturgeon sample MDX-3 and paddlefish specimen X-2724 were sampled up to the outermost growth increment.

Stable Isotope Analysis

Micromilled hydroxyapatite samples of ~50 μg were placed in Exetainer vials (Labco, Lampeter, UK) and flushed with purified helium gas. Orthophosphoric acid was subsequently added, which reacted for 24 hours at 45°C. Subsequently, the CO_2-He mixture of each sample

was directed into a cold trap where the CO_2 of the sample was frozen with liquid nitrogen for 2 minutes. After this 2-minute trapping, an accurate low-amplitude measurement was performed with a Thermo Finnigan Delta + mass spectrometer connected to a Thermo Finnigan GasBench II at the Earth Sciences Stable Isotope Laboratory (Vrije Universiteit, Amsterdam). This is repeated 3 times per sample vial.

Uncertainties for $\delta^{13}C$ were low, with a standard deviation of 0.28 ‰ of the Ag-Lox (modern elephant standard) for the micromilled samples in the cold trap.

Propagation Phase Contrast Synchrotron Radiation Micro Computed Tomography

Paddlefish specimen FAU.DGS.ND.161.4559.T, comprises an incomplete fish lacking the rostrum (paddle-shaped snout) and everything caudal to the pectoral girdle. FAU.DGS.ND.161.4559.T was collected during an earlier excavation by Robert DePalma and made available for PPC-SR µCT scanning. Data acquisition took place in May 2018 on Beamline BM05 at the European Synchrotron Radiation Facility, Grenoble, France. The entire specimen was scanned at 43.5 µm voxel size using the white beam of BM05 filtered with 0.4mm of molybdenum and 9mm of copper. The detector was based on a 2mm thick LuAG:Ce scintillator optically coupled to a PCO edge 4.2 CLHS sCMOS camera. The resulting average detected energy was then 132 keV. In order to obtain some propagation phase contrast, the distance between the sample and the detector was set at 5m. 205 scans, each of 5000 projections of 7ms were performed with a vertical displacement of 1.4mm for a vertical field of view of 2.8mm, ensuring a double scan of the complete samples. Scans were performed in half-acquisition mode to enlarge the lateral field of view. The volume was reconstructed using single distance phase retrieval algorithm coupled to filtered back-projection as implemented in the ESRF software PyHST2. Vertical concatenation, 16 bits conversion and ring artefacts corrections were performed using inhouse developed matlab scripts. Subsequently the gill region and impact spherules were scanned at 13.67 µm voxel size (0.4mm of molybdenum, 6mm of copper, LuAG:Ce scintillator of 500 microns, leading to detected energy of 166 keV,

propagation distance of 2.5m, two columns of 77 scans each of 4998 projections in half-acquisition with exposure time of 0.05s that were laterally concatenated after reconstruction). Furthermore, samples from the paddlefish dentaries and sturgeon pectoral fin spines were scanned at 4.35 µm voxel size for osteohistological analysis (3.5mm of Al, 11 bars of 5mm in diameter of Al, LuAG:Ce scintillator fo 500 µm, leading to a detected energy of 92 keV, propagation distance of 1.5m, one single column of 22 scans each of 4998 projections in half-acquisition with exposure time of 60 ms). Subsequent digital extraction of the bones and impact spherules were performed on VG Studio MAX 3.2. VG-studio MAX 3.2 additionally allowed for the creation of an artificial thin-section of the histological samples by using 'thick slab-mode', which can be created with the maximum, minimum, or average grey-values combined. These thin sections were produced at 0.1 mm thickness on average grey-values after careful 3D alignment of the volume in order to maximize the visibility of the annulus and lines of arrested growth (LAGs) and at 0.2 mm thickness on minimum grey-values in order to maximize the visibility of the osteocyte lacunae. All scanning data is available at the http://paleo.esrf.eu database.

Acknowledgements

MADD was partially funded by the European Association of Vertebrate Palaeontologists (EAVP) with the EAVP Research Grant (ERG). The ESRF is acknowledged for provisioning beamtime at BM05. Robert DePalma is thanked for inviting us to Tanis, making specimens available, and for proposing to study the season of the impact. We would like to thank Dr Koen Stein for accommodating us with the µXRF at the VUB in Brussels and the helpful discussions on bone histology. Dr Vincent Fernandez, and Dr Kimberley Chapelle helped with the segmentation in VG studio. Roel van Elsas for assistance on the SEM and

discussions on the resulting data. Bouke Lacet helped with the preparation of the thin and thick sections. Martine Hagen kindly allowed use of her sedimentology lab and the microbalance for weeks in a row. Dr Frank Peeters assisted in photographing the thin sections while sharing his thoughts on the project. We would like to thank Per Ahlberg for his advice, fruitful discussions, and identification of the brain and non-mineralized sidewalls of the cranial cavity. Finally, we are grateful for discussions with Phil Manning.

Author contributions

M.A.D.D., J.S., and H.J.L.v.d.L. conceived and designed the project. Materials were excavated by M.A.D.D. in 2017. M.A.D.D., D.F.A.E.V., C.B., and P.T. performed the synchrotron experiments. M.A.D.D. performed the XRF analysis and sampled the specimens with the micromill. M.A.D.D., S.V.W. and H.J.L.v.d.L performed the isotope analyses. P.T. processed and reconstructed the raw PPC-SRμCT scanning data. M.A.D.D., and D.F.A.E.V. segmented the scanning data. M.A.D.D., J.S., S.S., and H.J.L.v.d.L analysed the data. All authors discussed the interpretations. M.A.D.D. wrote the manuscript and created the figures and supplementary information with input from H.J.L.v.d.L., J.S., and D.F.A.E.V. All authors provided a critical review of the manuscript and approved the final draft.

Figure captions

Figure 1. a. Left lateral view of paddlefish FAU.DGS.ND.161.4559.T scanned at 43.5 μm voxel size, googly eye is indicating where its eye would roughly have been, square is indicating the location of the suboperculum (b). b. 13.67 μm voxel size segmentation of the suboperculum and gills with impact spherules (yellow). Scale bars are 2 cm. See supplementary information 3.2 for 2D synchrotron data and supplementary Video V1 for moving images of the 3D reconstruction.

Figure 2. Incremental growth profiles of Paddlefish X-2724. a, δ13C record (‰ VPDB). b, µCT 0.1 mm thick slab calculated by averaging 33 original slices (4.35 µm isotropic voxel size). c, µCT 0.2 mm thick slab calculated by minimizing 66 original slices (4.35 µm isotropic voxel size). d. Thin section under light microscopy with the Lines of Arrested Growth (LAGs). Arrows indicating LAGs at the final stage of the annulus (thin parallel lines) and just before the onset of the growth zones. All data are from the same specimen; b & c originate from a scan from approximately 1 cm below the cut thin section of c. Scale bars are 1 mm.

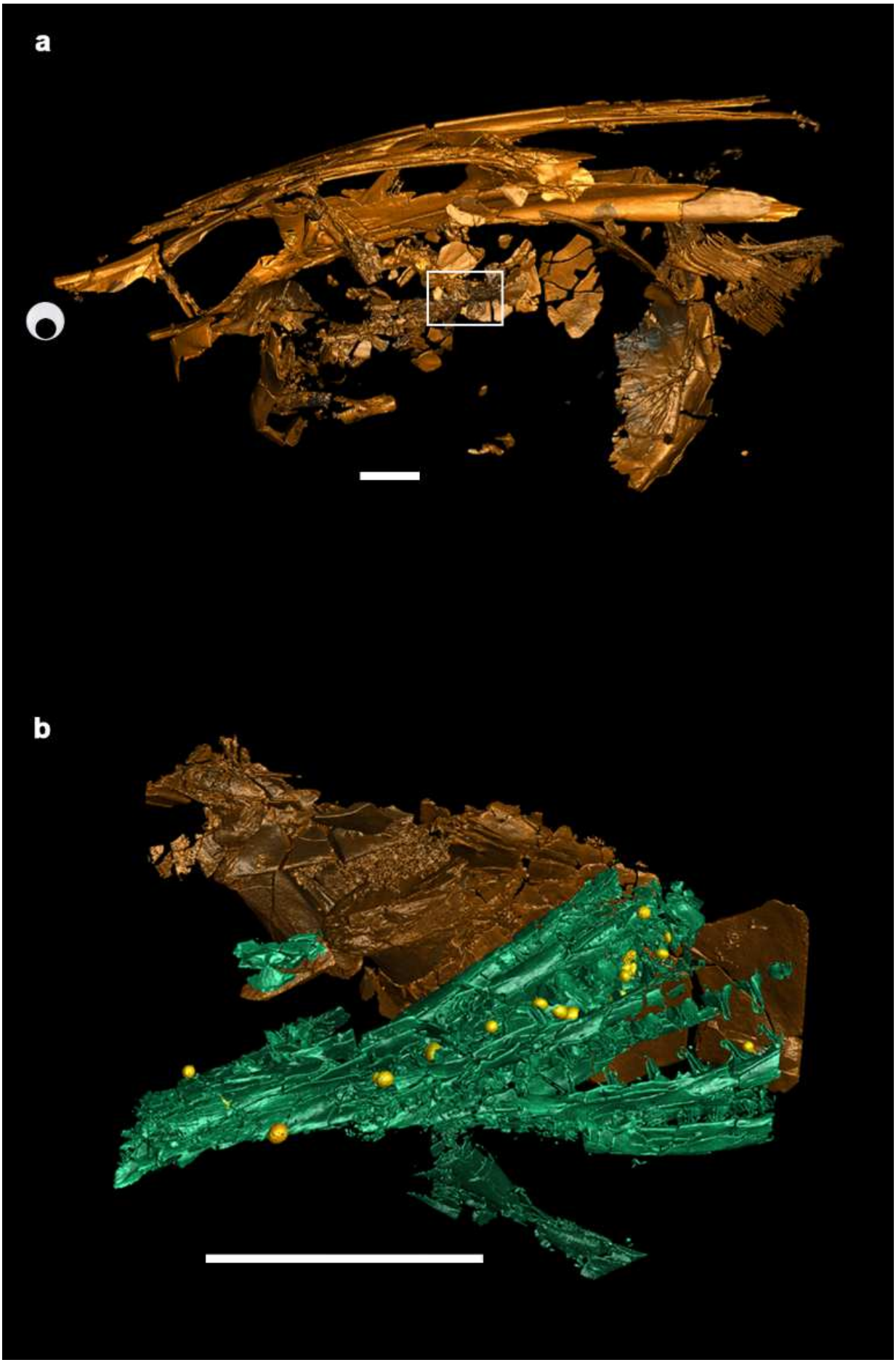

351

352

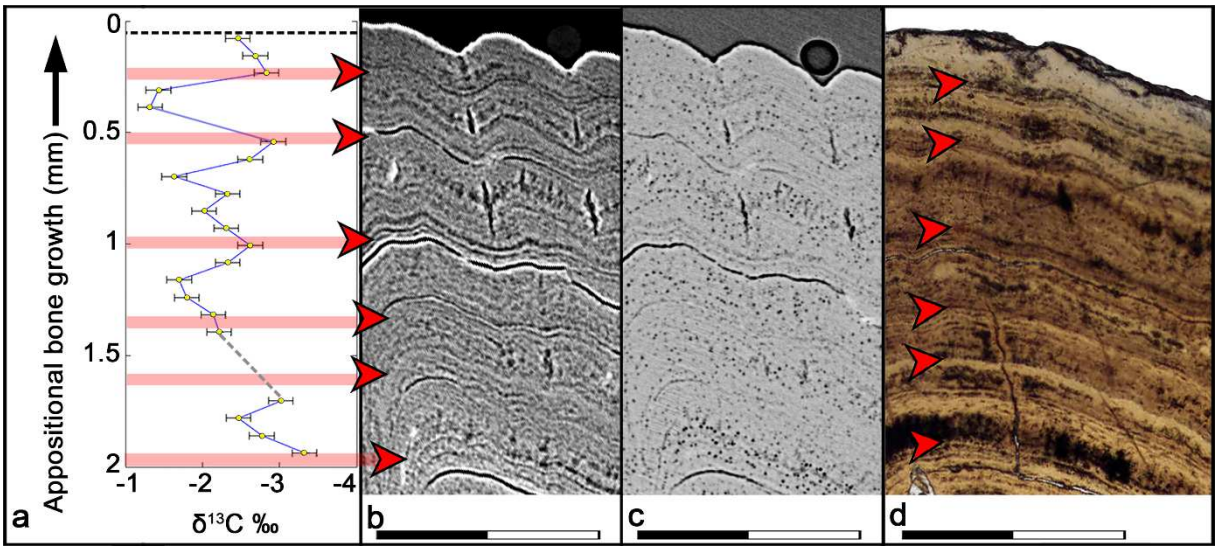

Supplementary Files

This is a list of supplementary files associated with this preprint. Click to download.

- V1.TanisPaddlefish.mp4
- Supplementaryinformation20210622submission.pdf